Indo-Pacific Warm Pool variability during the Holocene and Last Glacial Maximum

Jian Xu,[1,2] Wolfgang Kuhnt,[1] Ann Holbourn,[1] Marcus Regenberg,[1] and Nils Andersen[3]

Received 20 January 2010; revised 2 September 2010; accepted 22 September 2010; published 30 December 2010.

[1] We measured oxygen isotopes and Mg/Ca ratios in the surface-dwelling planktonic foraminifer *Globigerinoides ruber* (white s.s.) and the thermocline dweller *Pulleniatina obliquiloculata* to investigate upper ocean spatial variability in the Indo-Pacific Warm Pool (IPWP). We focused on three critical time intervals: the Last Glacial Maximum (LGM; 18–21.5 ka), the early Holocene (8–9 ka), and the late Holocene (0–2 ka). Our records from 24 stations in the South China Sea, Timor Sea, Indonesian seas, and western Pacific indicate overall dry and cool conditions in the IPWP during the LGM with a low thermal gradient between surface and thermocline waters. During the early Holocene, sea surface temperatures increased by ~3°C over the entire region, indicating intensification of the IPWP. However, in the eastern Indian Ocean (Timor Sea), the thermocline gradually shoaled from the LGM to early Holocene, reflecting intensification of the subsurface Indonesian Throughflow (ITF). Increased surface salinity in the South China Sea during the Holocene appears related to northward displacement of the monsoonal rain belt over the Asian continent together with enhanced influx of saltier Pacific surface water through the Luzon Strait and freshwater export through the Java Sea. Opening of the freshwater portal through the Java Sea in the early Holocene led to a change in the vertical structure of the ITF from surface- to thermocline-dominated flow and to substantial freshening of Timor Sea thermocline waters.

Citation: Xu, J., W. Kuhnt, A. Holbourn, M. Regenberg, and N. Andersen (2010), Indo-Pacific Warm Pool variability during the Holocene and Last Glacial Maximum, *Paleoceanography*, *25*, PA4230, doi:10.1029/2010PA001934.

1. Introduction

[2] The Indo-Pacific Warm Pool (IPWP) is the main source area of heat and water vapor export to the high latitudes, and thus plays a critical role in global climate [*Bjerknes*, 1969; *Webb et al.*, 1997; *Pierrehumbert*, 2000]. The size and intensity of the IPWP is closely linked to the El Niño-Southern Oscillation (ENSO), which strongly influences heat transport and thermocline depth in the western Pacific and eastern Indian Ocean [*Vranes et al.*, 2002; *Potemra et al.*, 2003]. During El Niño events, warm waters from the IPWP are driven eastward by strong westerly winds, resulting in reduced precipitation and shoaling of the thermocline within the IPWP as well as a weaker Indonesian Throughflow (ITF). El Niño-like conditions during the Last Glacial Maximum (LGM) would explain weaker zonal and meridional SST gradients in the equatorial Pacific [*Koutavas et al.*, 2002] and increased sea surface salinities at the northern margin of the IPWP close to Mindanao [*Stott et al.*, 2002]. In contrast, increased precipitation in the center of the IPWP and increased Pacific zonal SST gradients [*Lea et al.*, 2000] would support a La Niña state during the LGM. Glacial freshening of surface waters in the South China Sea (SCS) [*Oppo and Sun*, 2005] and Sulu Sea [*Oppo et al.*, 2003; *Rosenthal et al.*, 2003] suggested a seaward shift of monsoonal precipitation. Recently, *Oppo et al.* [2009] highlighted the role of the Asian monsoon/Intertropical Convergence Zone (ITCZ) in forcing precipitation anomalies in the IPWP on centennial-millennial timescales. Whether an El Niño or La Niña state prevailed within the IPWP region during the LGM and early Holocene remains an open question, which cannot be answered without improved spatial coverage of proxy records.

[3] The IPWP is also a key region connecting the Pacific and Indian Oceans via the ITF, and thus regulating salinity and heat budgets between these oceans [*Gordon and Fine*, 1996; *Gordon*, 2005]. It was initially suggested that restriction of the ITF (i.e., during glacial sea level lowstands) may have intensified the IPWP and cooled the Indian Ocean, which in turn may have weakened the Asian monsoon [*Lee et al.*, 2002]. However, recent oceanographic monitoring has shown that most of the ITF inflow originates from relatively cool and fresh North Pacific thermocline water [*Gordon*, 2005]. Today, the cool subsurface flow of the ITF becomes intensified relative to the warm surface flow by freshwater influx from the SCS to the Java Sea, which blocks the warm surface Makassar Strait outflow [*Gordon et al.*, 2003; *Tozuka et al.*, 2009]. Previous studies indicate that the vertical structure of the ITF probably varied considerably over precessional and glacial-interglacial timescales, with thermocline

[1]Institute of Geosciences, Christian Albrechts University, Kiel, Germany.
[2]Now at State Key Laboratory of Continental Dynamics and Department of Geology, Northwest University, Xi'an, China.
[3]Leibniz Laboratory for Radiometric Dating and Stable Isotope Research, Christian Albrechts University, Kiel, Germany.

0883-8305/10/2010PA001934

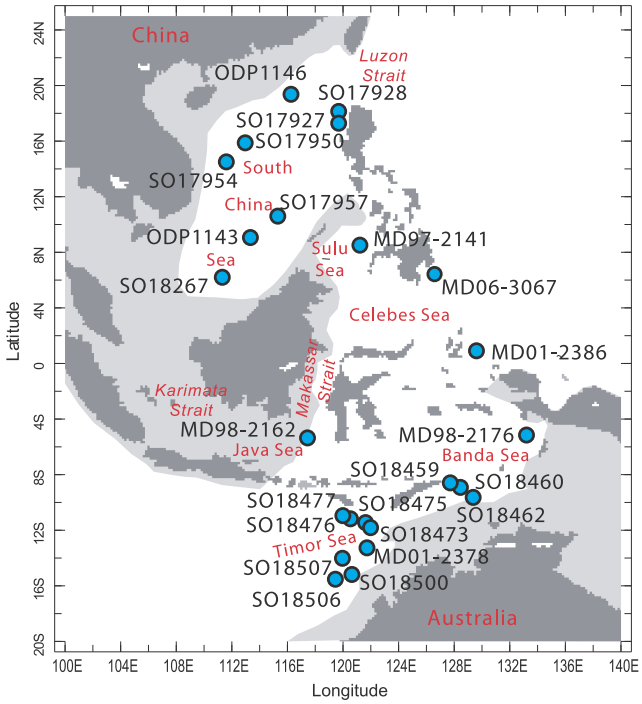

Figure 1. Locations of sediment cores investigated in the Indo-Pacific Warm Pool. Light gray shaded shelf areas were exposed during the LGM.

flow dominating during warm periods [*Žuvela*, 2005; *Xu et al.*, 2006, 2008].

[4] Previous SST and salinity reconstructions within the IPWP region mainly focused on the last Termination and the phasing of tropical SST with respect to global ice volume and high-latitude climate change [e.g., *Lea et al.*, 2000; *Kienast et al.*, 2001; *Koutavas et al.*, 2002; *Rosenthal et al.*, 2003; *Visser et al.*, 2003; *Stott et al.*, 2007; *Tachikawa et al.*, 2009]. These studies revealed an astonishing regional variability within the IPWP area and at its margins (northern SCS and Coral Sea). For example in the Makassar Strait, SST lead planktonic oxygen isotopes (interpreted as ice volume) by 2–3 kyr during Terminations I and II [*Visser et al.*, 2003], while in the Sulu Sea, southern SCS and Timor Sea (TS), SST are in phase with ice volume [*Kienast et al.*, 2001; *Rosenthal et al.*, 2003; *Xu et al.*, 2006]. However, a recent study, which focused on records in the Coral Sea supplemented by a compilation of ^{14}C-dated records from the Pacific during Termination I, indicated that the South and tropical Pacific started warming earlier than the North Pacific [*Tachikawa et al.*, 2009].

[5] Sea surface salinity reconstructions from the margin of the IPWP indicate a strong relation to Asian monsoon precipitation [e.g., *Rosenthal et al.*, 2003; *Oppo and Sun*, 2005; *Oppo et al.*, 2009] but the spatial coverage is still too sparse to fully resolve regional patterns. The coverage is even sparser for thermocline depth reconstructions. Little advance has been made since the pioneering work of *Andreasen and Ravelo* [1997] to reconstruct thermocline depth of the tropical Pacific for the LGM using transfer functions based on the distribution of tropical-subtropical planktonic foraminiferal assemblages. High-quality early Holocene to LGM data are especially lacking for the Australasian area and thermocline reconstructions based on multispecies Mg/Ca and oxygen isotope data are still in a preliminary stage for this area. Regional differences suggest that the intensity of the Australian monsoon and related changes in SST and productivity in the eastern Indian Ocean are not just a remote effect of the Asian winter monsoon. The Australian monsoon appears also to be directly forced by insolation over Australia with a dynamic feedback from ocean circulation patterns [*Liu et al.*, 2004]. In order to better understand the spatial heterogeneity of the IPWP records, which appears to depend strongly on the complex interactions of local monsoonal systems driven by insolation patterns, we also focus on the early Holocene, when precessional insolation was at a minimum over Australia.

[6] In this study, we reconstruct vertical water profiles in 24 sediment cores from the IPWP region based on two planktonic foraminiferal species, which live in different layers of the upper ocean water. Our main objective is to investigate changes in regional hydrology of the upper ocean during three time critical time slices: the late Holocene (0–2 ka), early Holocene (8–9 ka) and LGM (18–21.5 ka [*Sarnthein et al.*, 2003]) in order to better understand interactions between tropical climatic and Australian-Asian monsoonal systems, variations in the ENSO state and the spatial heterogeneity of the IPWP.

2. Materials and Methods

[7] Samples used in this study are mainly from sediment box, gravity, multi, piston and Kastenlot cores recovered during SONNE Cruises SO-95 (Monitor Monsoon) in 1994, SO-115 (Sundaflut) in 1996, and SO-185 (VITAL) in 2005, Images Cruises IV in 1998 (Indonesian Archipelago, western Pacific and East China Sea), VII (WEPAMA) in 2001 and XIV (Marco Polo II) and ODP Leg 184. These cores are located from 16°S–20°N to 110°E–140°E including the TS, SCS, Sulu Sea, Makassar Strait and the western Pacific (Figure 1 and auxiliary material Table S1).[1] We additionally used published oxygen isotope and Mg/Ca data from *Oppo et al.* [2003], *Rosenthal et al.* [2003], *Visser et al.* [2003], *Stott et al.* [2004] and *Xu et al.* [2008] (Table S1). To maintain coherency with our results, we used consistent calibration equations to convert published data to temperatures and $\delta^{18}O_{sw}$. Sediment samples processed in Kiel University were oven-dried below 40°C, disaggregated by soaking in water, then wet sieved over a 63 μm screen. Residues were dried on a sheet of filter paper below 40°C, then sieved into four different size fractions: 63–150 μm, 150–250 μm, 250–315 μm and >315 μm.

2.1. AMS ^{14}C Dating

[8] For accelerator mass spectrometry (AMS) ^{14}C dating, around 1300–1600 well-preserved shells of *Globigerinoides ruber* (white s.s.), weighing 7–13 mg, were picked from the size fraction 250–315 μm in 19 samples from Cores SO18460, SO18462, SO18473 and SO18475 (Table S2). As

[1] Auxiliary materials are available in the HTML. doi:10.1029/2010PA001934.

one sample from Core SO18473 had insufficient numbers of *G. ruber*, we used mixed planktonic foraminifers. AMS conventional ^{14}C ages were determined at the Leibniz Laboratory, Kiel University using standard methods described by *Schleicher et al.* [1998].

[9] AMS conventional ^{14}C ages were then converted to calendar ages following *Fairbanks et al.* [2005]. Before conversion, we corrected conventional ^{14}C by subtracting 300 years for reservoir age in TS [*Butzin et al.*, 2005]. Recent studies [*Sarnthein et al.*, 2007] have shown that glacial reservoir ages may be as high as 2000 years. However, even if we apply higher reservoir ages, converted ages for the LGM data set would remain older than 17.5 ka and still be representative for the late LGM and earliest termination. Conventional ^{14}C dates and calendar ages are shown in Table S2.

2.2. Stable Isotopes

[10] Approximately 45 tests of the near surface water dweller *G. ruber* and 30 tests of the upper thermocline species *Pulleniatina obliquiloculata* were picked from the size fraction 250–315 μm, then weighed and crushed. All tests were checked for cement encrustations and infillings before being crushed into fragments. Crushed tests were then mixed homogeneously and visually split into three aliquot parts. One part was used for stable isotope analysis and the other two parts for Mg/Ca analysis.

[11] For stable isotopes, crushed tests were cleaned in alcohol in an ultrasonic bath and dried at 40°C. Stable carbon and oxygen isotope measurements were made with the Finnigan MAT 251 mass spectrometer at the Leibniz Laboratory, Kiel University. The instrument is coupled online to a Carbo-Kiel Device (Type I) for automated CO_2 preparation from carbonate samples for isotopic analysis. Samples were reacted by individual acid addition. The mean external error and reproducibility (1σ) of carbonate standards is better than ±0.07‰ for $\delta^{18}O$. Results were calibrated using the National Institute of Standards and Technology (Gaithersburg, Maryland) carbonate isotope standard NBS 20 and in addition NBS 19 and 18, and are reported on the PeeDee Belemnite (PDB) scale. Sixty-eight replicates indicate that the mean reproducibility of foraminiferal samples is ±0.08‰ for $\delta^{18}O$. Individual measurements are listed in Table S3; mean $\delta^{18}O$ values for each time interval are given in Table S4.

[12] As several samples from Cores SO17927 and SO18267 had insufficient numbers of *G. ruber* and *P. obliquiloculata* from the size fraction 250–315 μm, we included tests from the smaller and larger size fractions (150–250 μm and >315 μm) for analysis. We checked the bias of shell size on stable isotopes in samples from Core SO18460. Comparison of 15 parallel measurements of *G. ruber* from the size fractions of 150–250 μm and >315 μm indicates a difference of 0.02 ± 0.12‰ and −0.01 ± 0.10‰ for $\delta^{18}O$ with measurements from the size fraction 250–315 μm. For *P. obliquiloculata*, 15 sets of parallel measurements from the size fractions >315 μm and 250–315 μm indicate a difference of 0.07 ± 0.18‰ for $\delta^{18}O$. The effect of shell size on $\delta^{18}O$ appears therefore to be negligible.

2.3. Mg/Ca Paleothermometry

[13] *G. ruber* is a well-known surface dweller, whereas *P. obliquiloculata* has a preferred depth habitat within the seasonal thermocline [*Xu et al.*, 2006; *Cléroux et al.*, 2007; *Farmer et al.*, 2007; *Mohtadi et al.*, 2009]. A study of 33 core top samples from the TS indicates that *P. obliquiloculata* Mg/Ca-based temperatures are generally comparable with WOA05 annual mean temperatures at water depth of 100–125 m [*Locarnini et al.*, 2006], supporting a thermocline depth habitat for this species [*Zuraida et al.*, 2009].

[14] Crushed tests were cleaned of contaminant phases using the standard foraminiferal cleaning procedure with reductive step [*Martin and Lea*, 2002]. Samples were analyzed on an ICP-OES (Spectro Ciros SOP) with cooled cyclonic spray chamber and microconcentric nebulization (200 μl min^{-1}) at the Institute of Geosciences, Kiel University. Intensity ratio calibration followed the method of *de Villiers et al.* [2002]. Internal analytical precision from replicate measurements is better than 0.1–0.2% (relative standard deviation), which corresponds to ±0.02°C. 31 replicate samples indicated sample reproducibility is ±2.5% or ±0.28°C for *G. ruber* and ±3.3% or ±0.37°C for *P. obliquiloculata*, respectively. The validity of Mg/Ca ratio for each sample was checked by evaluating the consistency of Ca concentration before and after cleaning. Samples with a reduction in Ca concentration of more than 20% were rejected. Fe/Ca, Al/Ca and Mn/Ca ratios were additionally used to monitor cleaning efficacy, and samples with a significant correlation between Fe/Ca, Al/Ca, Mn/Ca and Mg/Ca values were also rejected. Individual measurements are listed in Table S3; mean Mg/Ca values for each time interval are given in Table S4.

2.3.1. Effect of Carbonate Dissolution on Mg/Ca Ratio: Carbonate Dissolution Indices

[15] Mean shell weight is often used to effectively indicate the preservation state of planktonic foraminiferal shells [e.g., *Rosenthal and Lohmann*, 2002; *Visser et al.*, 2003; *Xu et al.*, 2006; *Tachikawa et al.*, 2008]. Planktonic foraminiferal fragmentation (expressed in % = (fragments/8)/(fragments/8+whole tests)*100 [*Le and Shackleton*, 1992]) has also been suggested as a reliable dissolution index [*Conan et al.*, 2002; *Barker et al.*, 2009]. In this study, we used mean shell weight, supplemented by the fragmentation based dissolution index above to evaluate carbonate dissolution (Table S5).

[16] We compared planktonic foraminiferal fragmentation (%) at five stations: ODP Site1146 [*Huang*, 2002], SO17957 [*Jian et al.*, 2000], ODP Site 1143 [*Xu*, 2004], MD98–2162 (this study) and MD01–2378 [*Xu et al.*, 2008]. Fragmentation is generally lower than 10% during the three studied time intervals, except at ODP Site 1146, where fragmentation reaches 10.5% during the early Holocene. Best preservation occurs in Cores MD98–2162 and MD01–2378, where fragmentation is 3% or less (Table S5).

[17] Mean shell weight of *G. ruber* ranges from ~10 to 20 μg and mean weight of *P. obliquiloculata* from ~12 to 19 μg. However, variability in *G. ruber* mean shell weight is less than 1 μg in most cores, except for Cores SO18459, SO18473, SO18475 and SO18500. Core SO18500 exhibits lower values during the late Holocene (12.1 ± 0.7 μg) than during the early Holocene (18.9 ± 0.1 μg) and LGM (18.6 ± 1.1 μg). In Cores SO18459, SO18473 and SO18475, highest values occur in the early Holocene and lowest values in the late Holocene.

[18] In contrast, *P. obliquiloculata* mean shell weight varies by less than 1.5 μg and exhibits no significant differences between the three time slices in most cores (Table S5). However, increasing downcore trends (>2.5 μg increase) from the late Holocene to LGM are evident in SCS Cores SO17954, SO17957 and ODP Site 1143 and in TS Cores SO18459, SO18460, SO18476 and SO1847. Since no such trend is detected in *G. ruber*, the decreasing trend from the LGM to Holocene does not appear to be related to carbonate dissolution.

2.3.2. Conversion of Mg/Ca to Temperature: Cleaning Protocol and Shell Size Effects

[19] Numerous calibration equations have been developed for converting planktonic foraminiferal Mg/Ca ratios into temperatures [e.g., *Barker et al.*, 2005, and references therein; *Huang et al.*, 2008; *Regenberg et al.*, 2009], either based on samples cleaned with or without a reductive step. According to *Rosenthal et al.* [2004], cleaning with a reductive step may lead to a decrease of up to ~15% in test Mg/Ca. To investigate the effect of reductive cleaning on *G. ruber* and *P. obliquiloculata*, we previously processed 41 duplicate samples with and without reduction between 451 cm and 891 cm in Core MD01–2378 [*Xu et al.*, 2008]. This revealed an average decrease in Mg/Ca of ~6.6% for *G. ruber* and of ~1.8% for *P. obliquiloculata* for tests cleaned with a reductive step [*Xu et al.*, 2008]. In this study, we therefore adjusted the Mg/Ca ratios of these two species accordingly for samples that were cleaned reductively (Table 1 and Table S4). These Mg/Ca losses translate into 0.7°C and 0.2°C, when converted into temperatures using standard calibrations with a 9% increase in Mg/Ca per °C.

[20] To convert Mg/Ca into temperature, we selected the species-specific calibration equations of *Anand et al.* [2003] (nonreductively cleaned) with a given accuracy of ±1.2°C. *Anand et al.* [2003] established two different species-specific *G. ruber* calibrations for the size fractions 350–500 μm and 250–350 μm, which both have the same slope but different intercepts. As a consequence, temperature estimates calculated with the *Anand et al.* [2003] calibration for size fraction 250–350 μm are consistently lower by ~1.4°C with respect to temperature estimates for the 350–500 μm calibration. To explore the effect of shell size on Mg/Ca ratios, we measured 15 duplicate samples from Core SO18460 from the size fractions 150–250 μm, 250–315 μm and >315 μm for *G. ruber* and from the size fractions 250–315 μm and >315 μm for *P. obliquiloculata*. Results show that *G. ruber* from the 150–250 μm size fractions have slightly less Mg/Ca (0.04 ± 0.15 mmol/mol) than *G. ruber* from the 250–315 μm size fraction, while *G. ruber* from the 250–315 μm size fraction and >315 μm fraction show no significant difference (0.00 ± 0.17 mmol/mol). This is in agreement with a recent core top assessment, which excluded large size-dependent variations in Mg/Ca ratios in species, which do not precipitate large amounts of gametogenic calcite such as *G. ruber* [*Ni et al.*, 2007]. Within the area of our study estimated Mg/Ca temperatures with the *G. ruber* 350–500 μm calibration of *Anand et al.* [2003] closely track temperatures at the sea surface, as indicated by the good fit between annual mean SSTs (WOA05 [*Locarnini et al.*, 2006]; Figure 2a) and 20 *G. ruber* core top Mg/Ca temperatures (~0.6 ± 0.5°C lower than annual average temperatures; Figure S1). Interestingly the *G. ruber* 250–350 μm calibration equation for the tropical Pacific of *Dekens et al.* [2002] is virtually identical to the 350–500 μm *G. ruber* calibration of *Anand et al.* [2003], indicating that the larger intercept of the 250–350 μm equation of *Anand et al.* [2003] may be a specific feature (related to seasonality?) of the Sargasso Sea, where this equation was developed.

[21] For *P. obliquiloculata*, Mg/Ca in the size fraction >315 μm also shows no systematic offset from the 250–315 μm fraction (0.00 ± 0.26 mmol/mol). We therefore assume that the effect of shell size on Mg/Ca is negligible. Measurements of 19 *P. obliquiloculata* core top samples yielded average Mg/Ca temperatures of 20.4 ± 1.5°C in the SCS, and 21.6 ± 0.7°C in the TS, which closely resemble annual seasonal temperatures at ~100 m water depth in these regions (Figure 2b).

2.3.3. Potential Salinity Bias on Mg/Ca Temperatures

[22] A recent study using core top material from the North Atlantic, Indian and Pacific Oceans [*Mathien-Blard and Bassinot*, 2009] suggested that the positive relationship between Mg/Ca in *G. ruber* and salinity is much stronger (15% Mg/Ca increase per psu) than previously assumed in culturing experiments (5% Mg/Ca increase per psu [*Kisakürek et al.*, 2008]). As a result *G. ruber* Mg/Ca temperature estimates based on the *Anand et al.* [2003] calibration for the size fraction 250–350 μm may underestimate calcification temperatures by ~1.6°C/psu, when salinity is lower than an average value of ~35.4 psu. However, this bias is strongly reduced, when using the *Anand et al.* [2003] calibration for the size fraction 350–500 μm, which results in generally 1.4°C higher temperature estimates. For this study we used the *Anand et al.* [2003] 350–500 μm size fraction calibration without salinity correction, as this produces the best correlation of regional core top SST estimates with local hydrologic data from WOA05 (Figure S1a). This approach is also consistent with the relatively low salinity bias observed in culturing experiments of 5% Mg/Ca increase per psu salinity increase [*Kisakürek et al.*, 2008]. Using a Mg/Ca calibration without salinity correction additionally reduces the problems associated with the application of a salinity correction for early Holocene and LGM data sets, where local hydrologic conditions (i.e., $\delta^{18}O$ of precipitation and the resulting $\delta^{18}O_{sw}$-salinity relationship) may have been different from today. Furthermore, regional high-resolution *G. ruber* Mg/Ca based temperature estimates without salinity correction result in consistent temperature patterns over the entire Indo-Pacific Warm Pool at least for the Holocene [*Linsley et al.*, 2010].

2.4. Calculation of Local Seawater $\delta^{18}O$ ($\delta^{18}O_{sw\text{-}corr}$)

[23] In a first step, we calculated surface and thermocline water oxygen isotope composition ($\delta^{18}O_{sw}$) by inserting Mg/Ca temperature and $\delta^{18}O$ values of *G. ruber* and *P. obliquiloculata* into the equation from *Bemis et al.* [1998]:

$$\delta^{18}O_{sw}(\mathrm{VSMOW}) = 0.27 + \left(T(^{\circ}\mathrm{C}) - 16.5 + 4.8 \times \delta^{18}O_{calcite(VPDB)}\right)/4.8. \quad (1)$$

[24] Seawater $\delta^{18}O$ is dependent on local seawater $\delta^{18}O$ (mainly related to salinity) and global ice volume or sea

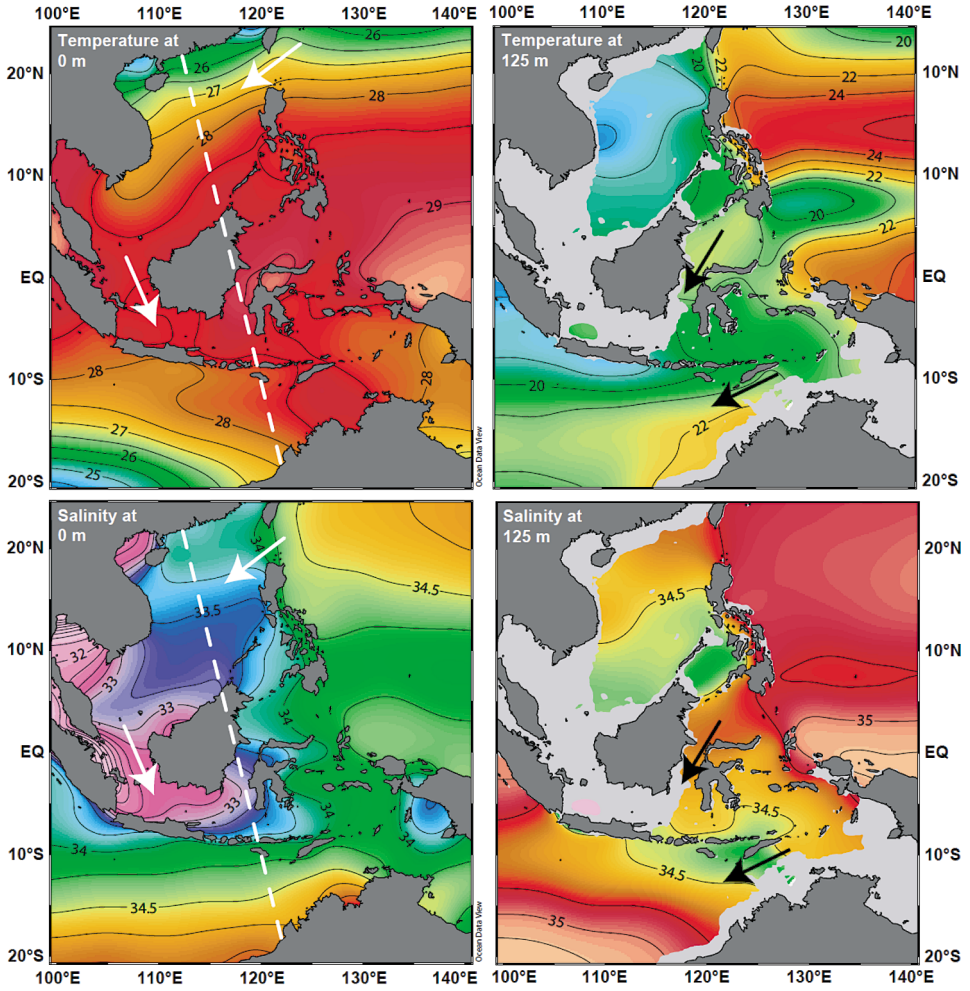

Figure 2a. Modern annual mean temperatures at (top left) 0 m and (top right) 125 m water depth and modern salinities at (bottom left) 0 m and (bottom right) 125 m water depth. White dashed line indicates transect AB from South China Sea to Timor Sea (112°E/23°N to 122.5E/19°S). White arrows indicate main flow paths of surface waters (SCS Throughflow); black arrows indicate main flow paths of thermocline waters (ITF). Data are from *Locarnini et al.* [2006]: http://iridl.ldeo.columbia.edu/SOURCES/.NOAA/.NODC/.WOA05/.Grid-1x1/.Annual/.an/.

level [e.g., *Waelbroeck et al.*, 2002]. To correct for ice volume, we deducted 0.21‰ from early Holocene values and 1.02‰ from LGM $\delta^{18}O_{sw}$ values [*Waelbroeck et al.*, 2002]. Since $\delta^{18}O_{rainwater}$ is relatively constant over the IPWP area [*Aleinov and Schmidt*, 2006], ice volume corrected $\delta^{18}O_{sw}$ ($\delta^{18}O_{sw\text{-}corr}$) mainly reflects local salinity. To test the reliability of our calculated $\delta^{18}O_{sw}$ (equation (1)), we present four salinity-$\delta^{18}O_{sw}$ relationships considering the effect of size fraction and salinity on Mg/Ca: temperature estimates following the *Anand et al.* [2003] calibrations for small/large size fractions and excluding/including salinity correction for Late Holocene Mg/Ca (Figure S2). In general, higher temperature estimates from the *Anand et al.* [2003] calibration equation for the size fraction 350–500 μm result in higher $\delta^{18}O_{sw}$ than when using the 250–350 μm calibration (see section 2.3.2). Application of the salinity correction to Mg/Ca also results in higher temperature estimates and hence $\delta^{18}O_{sw}$. As indicated by $\delta^{18}O_{sw}$ measurements from the TS (unpublished, SO185 cruise September 2005), two of the four $\delta^{18}O_{sw}$ scenarios reflect realistic values: (1) the large size-fraction calibrations without Mg/Ca-salinity correction and (2) the small size-fraction calibration combined with Mg/Ca-salinity correction. Since the correlation between salinity and $\delta^{18}O_{sw}$ is weak (r^2 = 0.38) for the latter, we favor the first approach (r^2 = 0.82) (Figures S2a and S2b). Local $\delta^{18}O_{sw}$ values are listed in Table S4.

3. Results

3.1. Age Models

[25] Age models for TS Cores MD01–2378 [*Holbourn et al.*, 2005; *Xu et al.*, 2008], SO18460, SO18462, SO18473 and SO18475 are based on AMS ^{14}C dates (Table S2). Average sedimentation rates in these cores are ~21 cm/kyr,

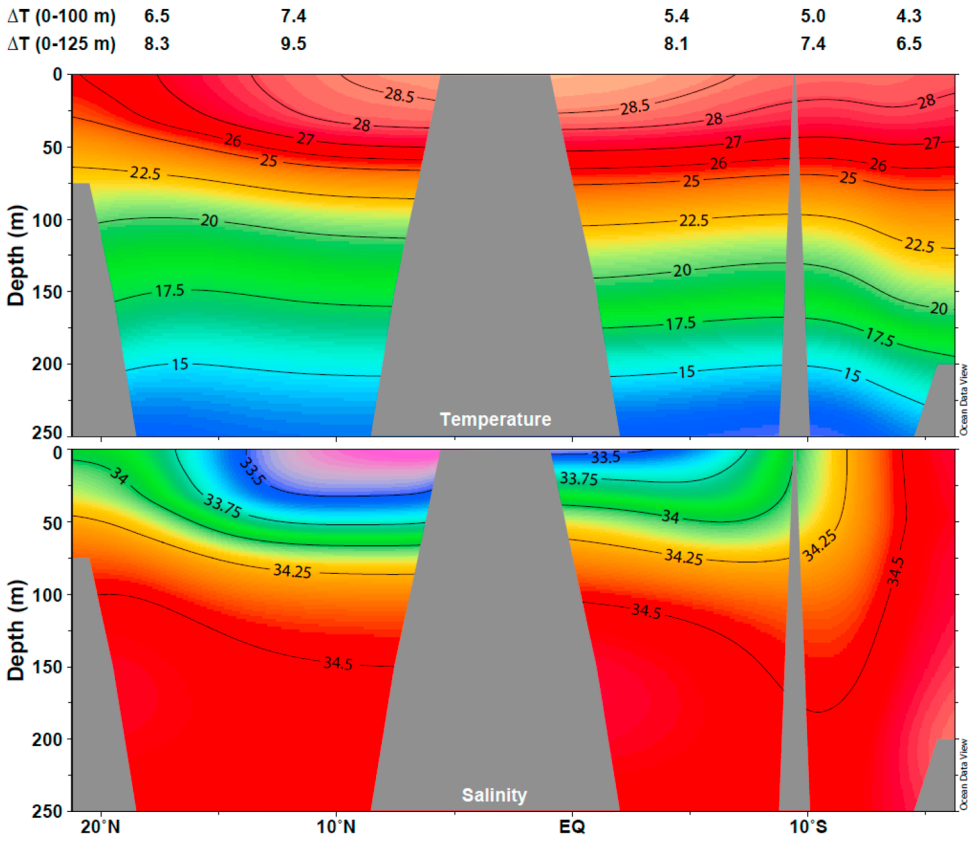

Figure 2b. Modern (top) temperature and (bottom) salinity profiles along transect AB from South China Sea to Timor Sea (112°E/23°N to 122.5E/19°S) as shown in Figure 2a.

~15 cm/kyr, ~22 cm/kyr, ~45 cm/kyr and ~41 cm/kyr; and their temporal resolutions are ~100 years, ~700 years, ~100 years, ~500 years and ~500 years, respectively. For TS Cores SO18459, SO18476, SO18477, SO184500, SO184506, SO184507, age models were generated from visual comparison of $\delta^{18}O$ curves with the $\delta^{18}O$ series in Core MD01–2378, which has a well-constrained age model based on 21 AMS ^{14}C dates [*Holbourn et al.*, 2005; *Xu et al.*, 2008] (Figure 3). References for published age models of SCS, Mindanao, Sulu Sea, Makassar and Banda Sea cores are given in Table S1.

3.2. Sea Surface and Upper Thermocline $\delta^{18}O$

[26] Mean $\delta^{18}O$ values at each site for the three time slices studied are listed in Table S4 and shown in Figure 4; mean regional $\delta^{18}O$ values are listed in Table 1. The late Holocene is characterized by relatively homogenous surface $\delta^{18}O$ (average −2.7‰) with slightly lower values (mean −2.90, stdev 0.33) in the SCS and slightly higher values in the western Pacific (mean −2.53‰, stdev 0.20). TS surface $\delta^{18}O$ is close to the modern regional average and quite homogenous (mean −2.70, stdev 0.06). In contrast to surface $\delta^{18}O$, there is a marked gradient in upper thermocline $\delta^{18}O$ between the SCS (mean 0.98‰, stdev 0.38) and the TS (mean −1.46‰, stdev 0.09). Off Mindanao and in the southern Makassar Strait, upper thermocline $\delta^{18}O$ values (−1.44‰ and −1.94‰, respectively) are close to or slightly lower than in the TS.

[27] Early Holocene surface $\delta^{18}O$ values are ~0.2‰ higher than in the late Holocene in the TS (mean −2.51, stdev 0.06) and western Pacific (mean −2.27‰, stdev 0.19), which probably reflects the isotopic effect of remaining ice caps. In contrast, early Holocene surface $\delta^{18}O$ values (mean −2.88‰, stdev 0.27) in the SCS are comparable to late Holocene values, implying a net increase by 0.2‰ from the early to late Holocene considering the isotopic effect of melting ice. Early Holocene upper thermocline $\delta^{18}O$ values retain the same gradient between the SCS (mean −0.82‰, stdev 0.37), TS and western Pacific (−1.35‰, stdev 0.07) with a consistent ice volume-related increase of 0.1–0.2‰.

[28] Sea surface hydrographic patterns were markedly different during the LGM with a strong contrast in surface $\delta^{18}O$ between the SCS (mean −1.63‰, stdev 0.40) and TS (mean −1.06‰, stdev 0.08), indicating a fresher and/or warmer glacial SCS surface. West Pacific values remain relatively close to TS values (mean −1.22‰, stdev 0.04). Upper thermocline $\delta^{18}O$ values were surprisingly homogenous during the LGM (0.14‰, stdev 0.37 in the SCS, 0.19‰ stdev 0.10 in the TS and 0.10‰ off Mindanao). In the SCS, there is virtually no LGM to Holocene change in sea level corrected thermocline $\delta^{18}O$, while glacial thermocline

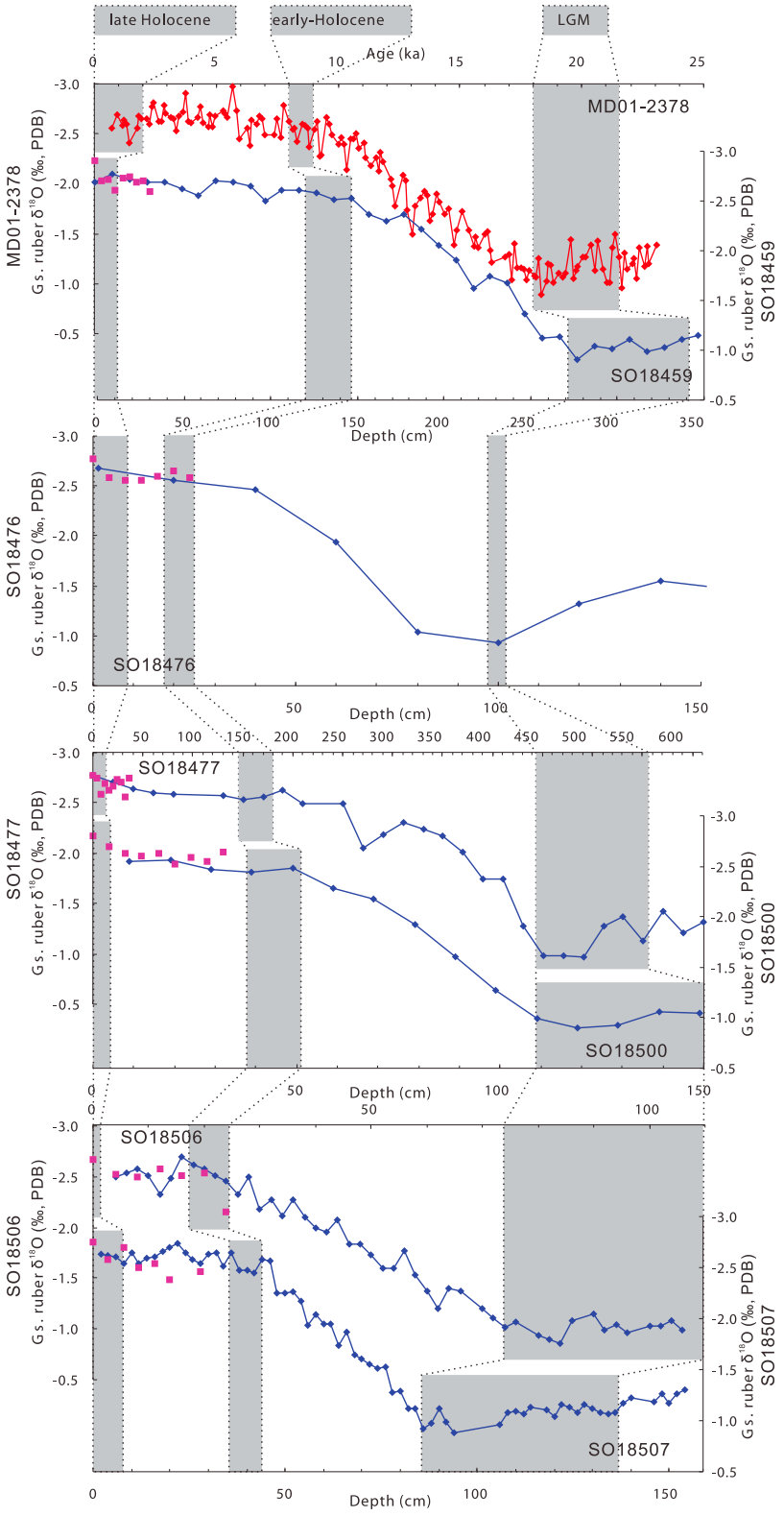

Figure 3. Comparison of *G. ruber* δ^{18}O versus depth in Cores SO18459, SO18476, SO18477, SO18500, SO18506, and SO18507 with *G. ruber* δ^{18}O in Core MD01-2378. Purple squares indicate multicorer samples. Grey shading marks late Holocene (0–2 ka), early Holocene (8–9 ka), and LGM (18–21.5 ka).

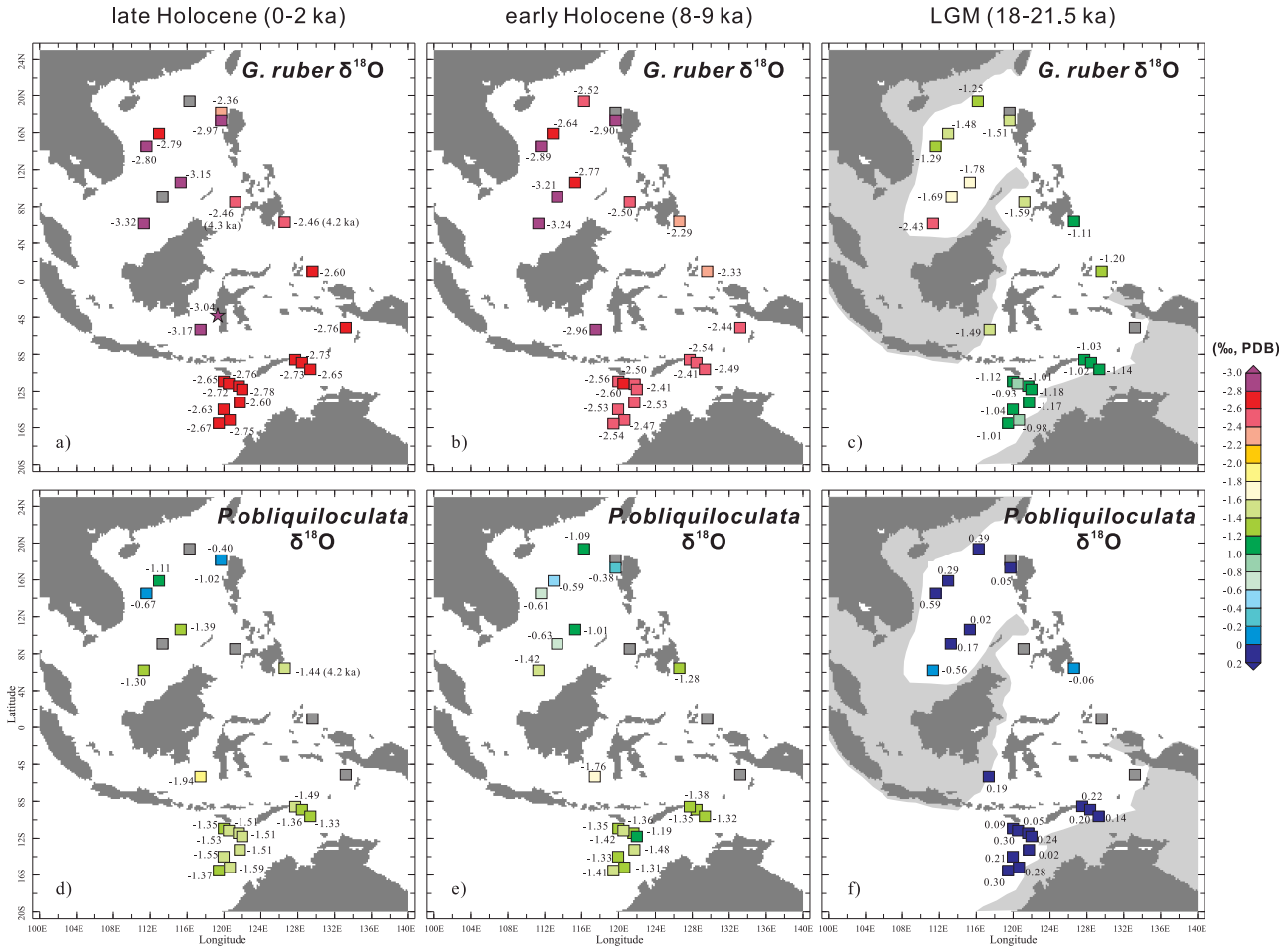

Figure 4. Regional distribution of *G. ruber* and *P. obliquiloculata* δ^{18}O (‰, PDB) during the late Holocene (0–2 ka), early Holocene (8–9 ka), and LGM (18–21.5 ka). Purple star indicates mean late Holocene value derived from *Oppo et al.* [2009]. During the LGM, there was a sharp contrast in surface δ^{18}O between the SCS and TS, whereas during the Holocene, the contrast in upper thermocline δ^{18}O became more accentuated.

δ^{18}O was on average 0.45‰ higher in the TS and West Pacific.

3.3. Sea Surface and Upper Thermocline Mg/Ca Temperatures

[29] Mean values of sea surface and upper thermocline temperatures at each site for the three time slices studied are listed in Table S4 and shown in Figure 5; mean regional SST values are listed in Table 2. During the late Holocene, a clear NW to SE gradient in SST is evident within the IPWP, as reflected by mean estimates of 26.8°C (stdev 0.45) in the SCS and of 28.0°C (stdev 0.59) in the TS. Western Pacific SST (28.1°C, stdev 0.78) are similar or slightly warmer than average TS estimates, and are close to modern annual SST in the IPWP [*Locarnini et al.*, 2006]. Reconstructed late Holocene upper thermocline temperatures exhibit a similar NW to SE warming trend (mean 20.4°C, stdev 1.48 in the SCS; mean 21.6°C, stdev 0.68 in the TS), which is in agreement with modern water temperatures at ~100 m water depth (~20.0°C in the SCS and ~22.5°C in the TS [*Locarnini et al.*, 2006]). However, upper thermocline temperatures exhibit relatively high variability overall, reflecting the influence of local monsoon related upwelling in the SCS and the impact of the ITF flow path in the Timor Strait and northern TS. Warmest upper thermocline temperatures (22.9 and 23.1°C) occur in the two central IPWP sites off Mindanao and in the southern Makassar Strait.

[30] Early Holocene average SSTs were slightly warmer than in the late Holocene in all basins, in particular within the TS, where mean SST was ~0.5°C warmer than today and in the late Holocene. In the SCS and western Pacific, changes in thermocline temperature appear quite negligible from the early to late Holocene, in contrast to the TS, where the mean temperature of 22.5°C (stdev 0.67) was clearly warmer by almost 1°C in the early Holocene than in the late Holocene.

[31] The glacial contrast in SST between the SCS and the TS is relatively small (SCS mean: 24.3°C, stdev 1.36; TS: 25.5°C, stdev 0.76 and western Pacific: 25.2°C, stdev 1.19).

Table 1. Regional Mean Values of Oxygen Isotopes and Mg/Ca Ratios During the Late Holocene (LH, 0–2 ka), Early Holocene (EH, 8–9 ka), and Last Glacial Maximum (LGM, 18–21.5 ka)[a]

	$\delta^{18}O$ *G. ruber*	Mg/Ca *G. ruber*	Mg/Ca *G. ruber* Corrected for Cleaning (+6.6%)	T *G. ruber* After *Anand et al.* [2003] After Cleaning Correction	$\delta^{18}O$ *P. obliquiloculata*	Mg/Ca *P. obliquiloculata*	Mg/Ca *P. obliquiloculata* Corrected for Cleaning (+1.8%)	T *P. obliquiloculata* After *Anand et al.* [2003] After Cleaning Correction	T *G. ruber* - T *P.obliquiloculata*	$\delta^{18}O_{sw\text{-}corr}$ *G. ruber*	$\delta^{18}O_{sw\text{-}corr}$ *P. obliquiloculata*
						Late Holocene					
Mean SCS	−2.90	4.15	4.42	26.83	−0.98	2.03	2.07	20.37	6.94	−0.48	−0.01
Stdev SCS	0.33	0.17	0.18	0.45	0.38	0.29	0.29	1.48	0.79	0.27	0.22
Number of sites	6	6	6	6	6	7	7	7	6	6	6
Mean Timor Sea	−2.70	4.57	4.93	28.04	−1.46	2.25	2.29	21.56	6.48	−0.02	−0.14
Stdev Timor Sea	0.06	0.25	0.26	0.58	0.09	0.14	0.14	0.68	0.78	0.13	0.11
Number of sites	11	11	11	11	11	11	11	11	11	11	11
Mean W-Pacific	−2.53	4.66	4.97	28.11	−1.44	2.54	2.58	22.94	4.74	0.08	0.17
Stdev W-Pacific	0.20	0.33	0.36	0.78	n.d.	n.d.	n.d.	n.d.	n.d.	0.08	n.d.
Number of sites	4	3	3	3	1	1	1	1	1	3	1
						Early Holocene					
Mean SCS	−2.88	4.18	4.46	26.93	−0.82	2.00	2.04	20.15	6.78	−0.65	0.00
Stdev SCS	0.27	0.17	0.19	0.46	0.37	0.39	0.39	1.92	1.69	0.26	0.44
Number of sites	7	7	7	7	7	7	7	7	7	7	7
Mean Timor Sea	−2.51	4.76	5.15	28.50	−1.35	2.43	2.48	22.45	6.05	0.05	−0.06
Stdev Timor Sea	0.06	0.33	0.41	0.90	0.07	0.15	0.15	0.67	0.82	0.21	0.16
Number of sites	11	11	11	11	11	11	11	11	11	11	11
Mean W-Pacific	−2.27	4.78	5.03	28.21	−1.35	2.47	2.52	22.65	6.27	0.20	−0.01
Stdev W-Pacific	0.19	0.56	0.57	1.29	n.d.	n.d.	n.d.	n.d.	n.d.	0.18	n.d.
Number of sites	6	5	5	5	1	1	1	1	1	5	1
						LGM					
Mean SCS	−1.63	3.31	3.53	24.26	0.14	1.71	1.74	18.48	5.78	−0.77	−0.20
Stdev SCS	0.40	0.42	0.45	1.36	0.37	0.16	0.16	1.03	0.90	0.27	0.23
Number of sites	7	7	7	7	7	7	7	7	7	7	7
Mean Timor Sea	−1.06	3.67	3.94	25.53	0.19	2.16	2.19	21.08	4.45	0.07	0.39
Stdev Timor Sea	0.08	0.27	0.28	0.76	0.10	0.20	0.20	1.02	0.85	0.15	0.19
Number of sites	11	11	11	11	11	11	11	11	11	11	11
Mean W-Pacific	−1.22	3.66	3.84	25.21	0.10	2.21	2.25	21.40	5.19	−0.16	0.37
Stdev W-Pacific	0.04	0.37	0.41	1.19	n.d.	n.d.	n.d.	n.d.	n.d.	0.27	n.d.
Number of sites	5	4	4	4	1	1	1	1	1	4	1

[a]Local seawater $\delta^{18}O$ ($\delta^{18}O_{sw\text{-}corr}$) is calculated from $\delta^{18}O$ values and Mg/Ca temperatures, using the Orbulina LL equation $\delta^{18}O_{sw}$ (VSMOW) = 0.27 + (T(°C) – 16.5 + 4.8 × $\delta^{18}O_{calcite(VPDB)}$)/4.8 from *Bemis et al.* [1998] and subtracting an ice volume effect of 0.21‰ for EH and 1.02‰ for LGM [*Waelbroeck et al.*, 2002].

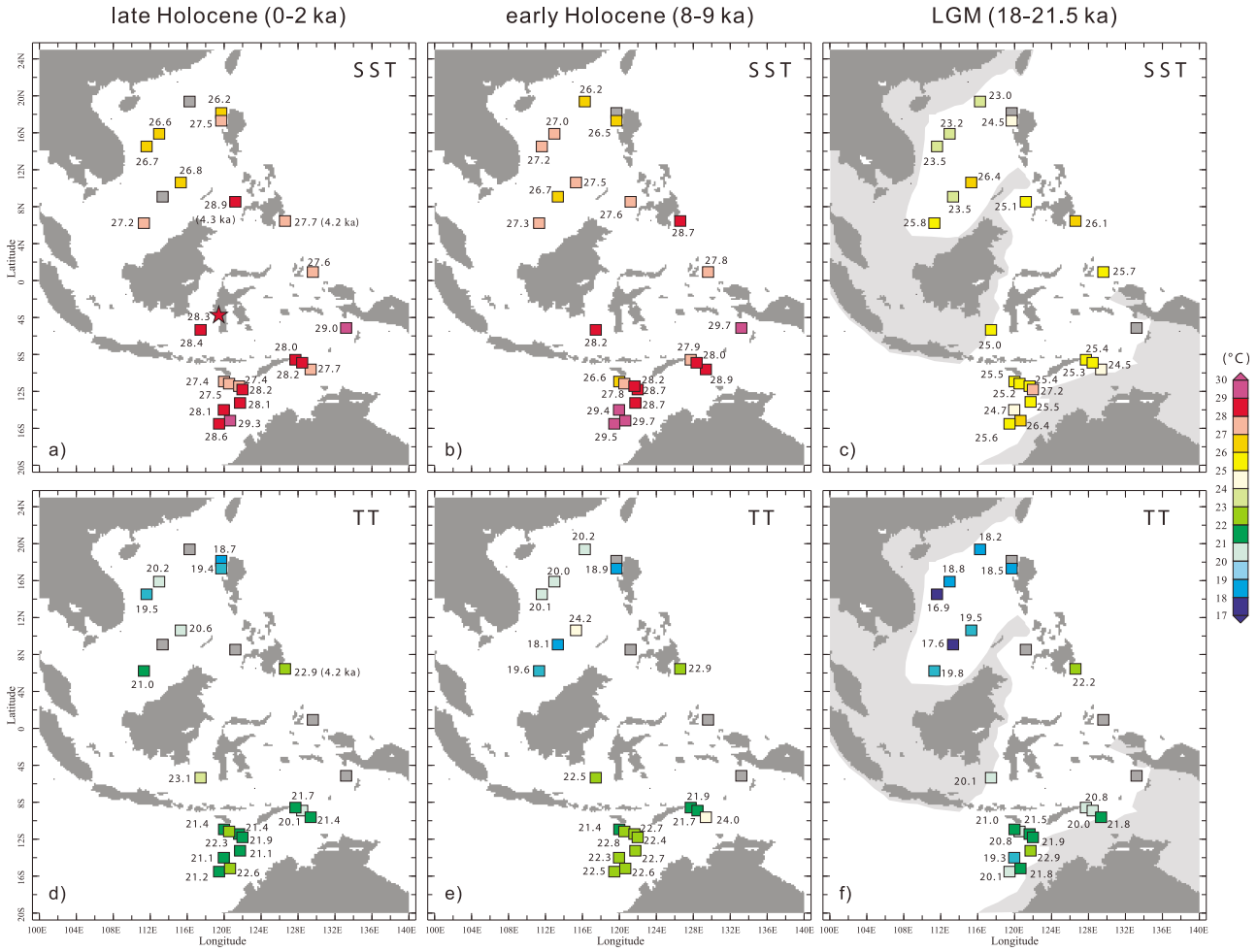

Figure 5. Regional surface and thermocline temperatures (°C) during late Holocene (0–2 ka), early Holocene (8–9 ka), and LGM (18–21.5 ka). During the LGM, there was a sharp contrast in upper thermocline temperatures between the SCS and TS, as relatively warm and salty Indian Ocean upper thermocline waters dominated in the TS. During the Holocene, SST increased by ~3°C over the entire IPWP region, suggesting intensification of the IPWP.

Deglacial warming was fairly consistent over the entire IPWP region and the N-S gradient (~1.3°C) remained close to the present-day average (Table 2). In contrast, the difference in upper thermocline mean temperatures between the SCS (mean 18.5°C, stdev 1.03) and the TS (mean 21.1°C, stdev 1.02) was enhanced (~2.6°C) during the LGM.

[32] The thermal gradient (ΔT) between SST and upper thermocline temperatures differs markedly in the SCS and TS for each of the three time slices investigated (Figure 6). Average ΔTs are 6.4°C, stdev 0.8 and 5.8°C, stdev 0.7 during the late Holocene, 6.3°C, stdev 1.7 and 5.4°C, stdev 0.7 during the early Holocene, and 5.3°C, stdev 0.9 and 3.9°C, stdev 0.8 during the LGM in the SCS and TS, respectively. The change in ΔT from the LGM to early Holocene is relatively small (~1.1°C) in the SCS, whereas it is more pronounced (~1.9°C) in the TS. Within a stratified upper water column, the thermal gradient is inversely related to the depth of thermocline: a steep gradient (up to 8°C in the SCS) indicates a shallow thermocline, whereas a low gradient (around 5–6°C in the western Pacific and TS) indicates a deep thermocline. However, low thermal gradients (below 5°C) in combination with relatively cool local SST may be due to enhanced mixing within the upper water column, as for instance in the late Holocene and LGM off Mindanao (Core MD06–3067), in the early Holocene in the

Table 2. Comparison of Mean Glacial, Early Holocene, and Late Holocene Mg/Ca Derived SST in the IPWP[a]

	SCS	Timor Sea	West Pacific/ Makassar
Late Holocene	26.83 (0.45)	28.04 (0.85)	28.11 (0.78)
Early Holocene	26.93 (0.46)	28.50 (0.90)	28.21 (1.29)
LGM	24.26 (1.36)	25.53 (0.76)	25.21 (1.19)
Early to late Holocene cooling	0.10	0.46	0.10
Deglacial warming	2.67	2.97	3.00

[a]Given in °C with standard deviations in parentheses.

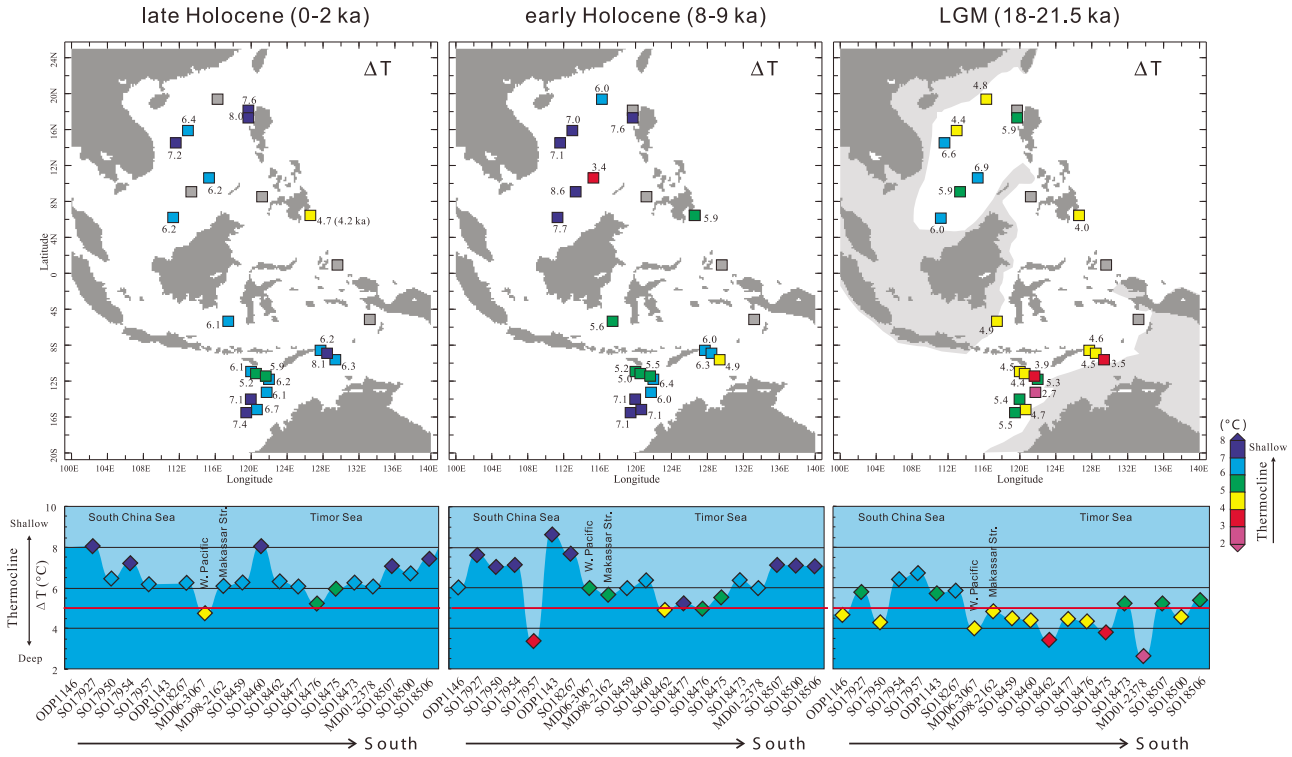

Figure 6. Thermal gradient (ΔT) between surface and thermocline waters (°C) during late Holocene (0–2 ka), early Holocene (8–9 ka), and LGM (18–21.5 ka). The bottom panels show ΔT distributions along N-S transects for the three time slices. During the Holocene, substantial shoaling of the thermocline occurred in the TS, as freshwater export from the SCS altered the ITF vertical structure from surface- to thermocline-dominated flow downstream of the Makassar Strait.

SCS (Core SO17957) and at the LGM in the TS (Cores SO18462, 18475 and MD01–2378).

3.4. Local Seawater $\delta^{18}O$ ($\delta^{18}O_{sw\text{-}corr}$)

[33] Mean $\delta^{18}O_{sw\text{-}corr}$ values at each site for the three time slices studied are listed in Table S4 and shown in Figure 7; mean regional $\delta^{18}O_{sw\text{-}corr}$ values are listed in Table 1. Late Holocene reconstructed surface $\delta^{18}O_{sw\text{-}corr}$ values exhibit a clear NW to SE gradient from the SCS (mean −0.48‰, stdev 0.27) to the center of the IPWP (mean 0.08‰, stdev 0.08) and to the TS (mean 0.02‰, stedv 0.13). This pattern closely resembles present-day sea annual average surface salinities, which range between 33 psu and 33.8 psu in the SCS, and increase to 34.2–34.6 psu in the TS (Figure 2). Interestingly, surface $\delta^{18}O_{sw\text{-}corr}$ values at the southern end of the Makassar Strait (−0.33‰ and −0.41‰) are closer to southern SCS than to TS values. This trend is not reflected in upper thermocline $\delta^{18}O_{sw\text{-}corr}$, which in sharp contrast to surface $\delta^{18}O_{sw\text{-}corr}$ is lower in the TS (mean −0.14‰, stdev 0.11) than in the SCS (mean −0.01‰, stdev 0.22). Highest late Holocene upper thermocline $\delta^{18}O_{sw\text{-}corr}$ values occur at SCS Site SO17928, NW of Luzon and Site MD01–3967, off Mindanao in the open tropical western Pacific. Both sites are located in areas affected by winter monsoon driven upwelling, which may pump deeper, more saline water to the upper thermocline.

[34] During the early Holocene, the sea surface $\delta^{18}O_{sw\text{-}corr}$ gradient between the SCS and TS was more intensified (mean −0.65‰, 0.26 stdev in the SCS; mean 0.05‰, 0.21 stdev in the TS). In contrast, early Holocene upper thermocline $\delta^{18}O_{sw\text{-}corr}$ values are close to late Holocene values (mean 0.00‰, stdev 0.44 in the SCS; mean −0.06‰, stdev 0.16 in the TS). As in the late Holocene, upper thermocline $\delta^{18}O_{sw\text{-}corr}$ show high variability, which may be related to local upwelling.

[35] Glacial mean sea surface $\delta^{18}O_{sw\text{-}corr}$ values in the SCS (mean −0.77‰, stdev 0.27) were close to early Holocene values. The overall fresh and homogenous sea surface in the glacial SCS probably arises from the more enclosed nature of this estuarine marginal basin during the LGM. In the TS, there is little LGM to Holocene contrast in surface $\delta^{18}O_{sw\text{-}corr}$ with a glacial mean $\delta^{18}O_{sw\text{-}corr}$ of 0.07‰, stdev 0.15. However,

Figure 7. Distribution of seawater $\delta^{18}O$ corrected for ice volume ($\delta^{18}O_{sw\text{-}corr}$) (corrections are late Holocene 0‰, early Holocene 0.21‰, and LGM 1.02‰ following *Waelbroeck et al.* [2002]) in surface and thermocline waters. During the Holocene, freshwater export from the Java Sea fundamentally altered the ITF upper profile and led to substantial freshening of TS upper thermocline waters.

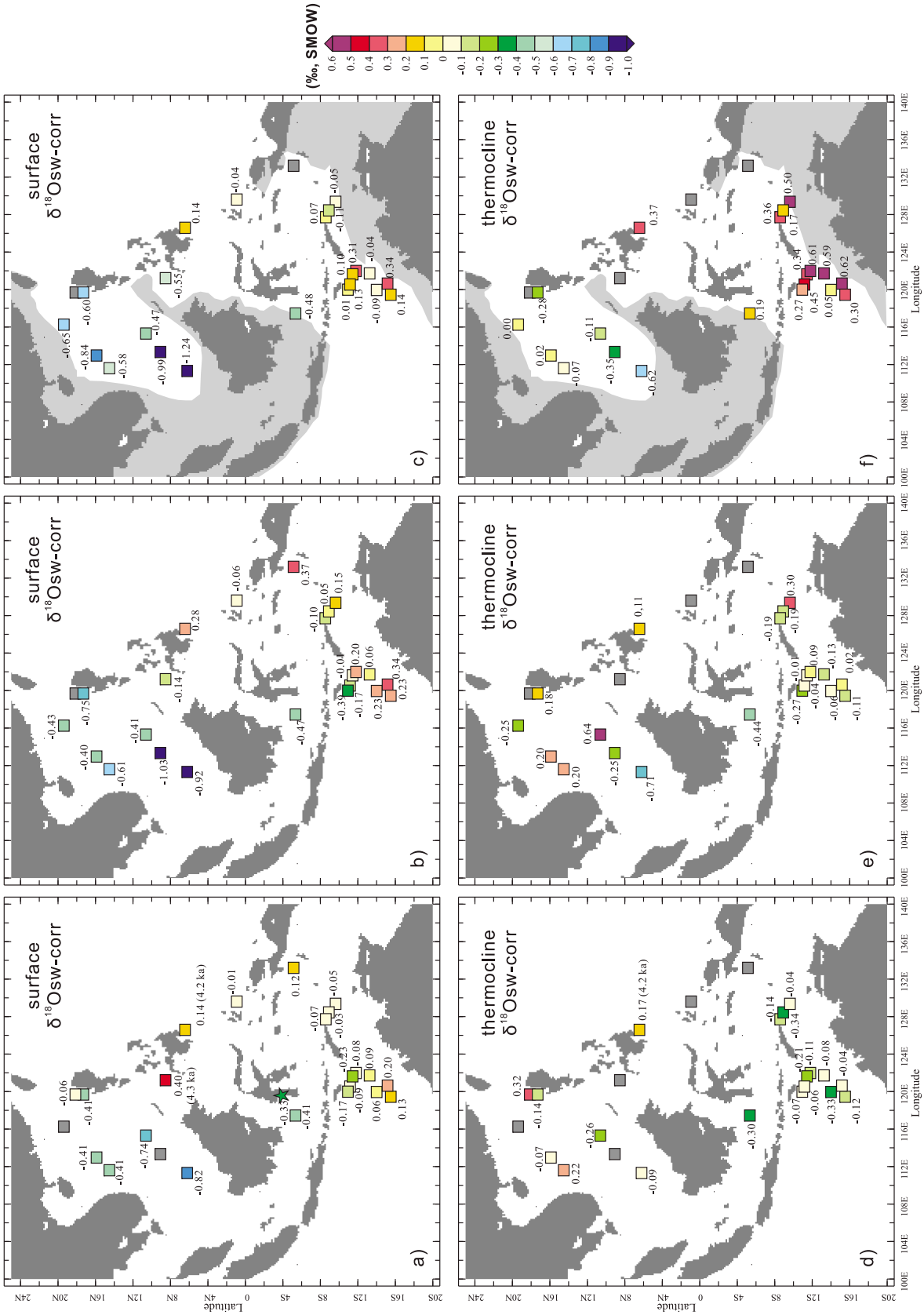
late Holocene (0-2 ka)
early Holocene (8-9 ka)
LGM (18-21.5 ka)
surface δ18Osw-corr
thermocline δ18Osw-corr
(‰, SMOW)
0.6 0.5 0.4 0.3 0.2 0.1 0 -0.1 -0.2 -0.3 -0.4 -0.5 -0.6 -0.7 -0.8 -0.9 -1.0
a)
b)
c)
d)
e)
f)
0.14 (4.2 ka)
0.40 (4.3 ka)
0.17 (4.2 ka)
Latitude
Longitude

Figure 7

glacial upper thermocline $\delta^{18}O_{sw\text{-}corr}$ values were considerably higher in the TS (mean 0.39‰, 0.19 stdev), whereas glacial values in the SCS remained similar to Holocene values (−0.20‰, 0.23 stdev).

4. Discussion

4.1. Salinity Contrast Between the SCS and Indonesian Seas

[36] Today, the SCS is a main heat and freshwater conveyor, as it provides a major pathway for surface waters flowing from the West Pacific into the Indonesian Seas [*Qu et al.*, 2009]. Surface waters remained significantly fresher in the SCS than in other regions of the IPWP during the Holocene (Figure 7). This regional contrast was further enhanced during the LGM, as SCS $\delta^{18}O_{sw\text{-}corr}$ was lower than in the Holocene and TS $\delta^{18}O_{sw\text{-}corr}$ was slightly higher (Figure 7). The gradual freshening in TS surface and thermocline waters during the late and early Holocene is probably linked to enhanced freshwater export from the southern SCS through the Java Sea. Today, instrumental data and modeling experiments show that a significant freshwater export flow from the SCS occurs through the Karimata Strait (Figure 2a) [*Gordon et al.*, 2003; *Tozuka et al.*, 2007, 2009]. As a result, the main annual average ITF transport into the Indian Ocean occurs in the upper thermocline and carries a large amount of SCS derived freshwater. In contrast, when the SCS influx is shut off, ITF transport shifts toward the surface, and the outflow becomes overall saltier [*Tozuka et al.*, 2007]. Today, a reduction in freshwater flux from the SCS occurs seasonally during boreal summer, when southwesterly monsoonal winds inhibit the export flow through the Java Sea. During the LGM, a saltier and surface-dominated ITF prevailed, as the Sunda Shelf was exposed and the freshwater export through the Karimata Strait was cut off. Freshwater influx from the SCS resumed in the later part of Termination I (~9.5 ka) [*Xu et al.*, 2008; *Linsley et al.*, 2010], when sea level reached a critical threshold of −30 to −40 m [*Lambeck and Chappell*, 2001], corresponding to the sill depth of the Karimata Strait.

[37] The glacial shut off of freshwater export through the Karimata Strait probably also had repercussions on the heat and salinity budgets of the SCS. *Wei et al.* [2003] attributed low *G. ruber* $\delta^{18}O$ values in the SCS to increased river discharge of freshwater into the SCS and enhanced summer monsoon precipitation. This scenario is supported by the distribution of surface water $\delta^{18}O_{sw\text{-}corr}$ during the Holocene and LGM in the SCS (Figure 7). Although monsoon-related precipitation and river discharge of freshwater may account for the SW-NE increase in surface water salinities within the SCS [e.g., *Wang et al.*, 1999; *Wei et al.*, 2003; *Cheng et al.*, 2005], they cannot however explain the increase in surface $\delta^{18}O_{sw\text{-}corr}$ with time (Figure 7). A semienclosed glacial SCS, with the Luzon Strait as the only significant connection to the open Pacific, may have developed a positive precipitation-runoff to evaporation balance due to summer monsoon rainfall and freshwater input from the Mekong, Red and Pearl Rivers. The relatively fresh surface and thermocline waters in the SCS during the LGM (Figure 7) may reflect this estuarine circulation pattern. In the early to late Holocene, increased freshwater export across the Sunda Shelf and enhanced flow of relatively cooler and saltier NW Pacific waters into the SCS through the Luzon Strait probably favored a more vigorous interbasinal circulation through the SCS, as suggested by surface and thermocline temperatures and $\delta^{18}O_{sw\text{-}corr}$ data (Figures 5 and 7).

4.2. ENSO Influence on IPWP Upper Ocean Variability?

[38] Contraction and expansion of the IPWP are characteristic features of ENSO-related climate variability, and exert a major influence on precipitation over the western tropical Pacific. At the end of the last glacial, surface waters show an overall increase of ~2.5–3.0°C (Figure 5), indicating expansion or intensification of the IPWP. Relatively fresh ($\delta^{18}O_{sw\text{-}corr}$ < 0‰) and warm (>28°C) waters dominated the western part of the IPWP region during the early Holocene consistent with precipitation patterns during the La Niña phase of ENSO (Figures 5 and 7). Pacific climate records and modeling experiments indicate that El Niño events were less frequent during the early Holocene [*Wells*, 1990; *Rodbell et al.*, 1999; *Liu et al.*, 2000; *Sandweiss et al.*, 2001; *Moy et al.*, 2002; *Loubere et al.*, 2003; *Marx et al.*, 2009]. Reduced ENSO activity in the early Holocene was related to intensification of the Asian summer monsoon and subduction of South Pacific warm waters into the equatorial thermocline. Intensified Asian summer monsoon during the early Holocene is suggested by $\delta^{18}O$ records in stalagmites from the Dongge Cave [*Yuan et al.*, 2004], and by evidence for northward displacement of the ITCZ [*Haug et al.*, 2001; *Tierney and Russell*, 2007; *Fleitmann et al.*, 2007; *Yancheva et al.*, 2007; *Tierney et al.*, 2010]. All of these factors would influence regional hydrology in the same direction, resulting in a northwestward shift and expansion of the "rain pool" in the early Holocene.

[39] However, the spatial pattern of LGM surface $\delta^{18}O_{sw\text{-}corr}$ deviations from modern values bears little resemblance to modern El Niño rainfall anomalies [*Dai and Wigley*, 2000; *Chen et al.*, 2004]. The strongest deviation, a massive glacial freshening in the southern SCS (up to 0.4‰ lower $\delta^{18}O_{sw\text{-}corr}$ values), occurs in an area with reduced annual precipitation during El Niño years. This freshening may be partly explained by increased glacial runoff from the Molengraaff and Paleo-Mekong rivers due to a seaward shift of the coastline and weakening of summer-monsoon-driven upwelling off Vietnam. Glacial freshening (0.4 to 0.9‰ lower $\delta^{18}O_{sw\text{-}corr}$; Figure 7) occurs also in the northern SCS, which today shows little ENSO-related precipitation change. Furthermore, glacial and Holocene $\delta^{18}O_{sw\text{-}corr}$ values remain virtually identical in the central part of the IPWP (Mindanao, Makassar, Banda Sea), where El Niño related precipitation anomalies are strongest today. In conclusion, the glacial-interglacial changes in $\delta^{18}O_{sw\text{-}corr}$ within the IPWP exhibit a distinctly different pattern than modern ENSO related precipitation anomalies, which suggests that ENSO variability cannot be used as a template to account for hydrological changes in the IPWP.

4.3. Impact of ITF on Timor Sea Hydrology

[40] Today the ITF transports relatively cool and fresh thermocline waters of North Pacific origin into the tropical Indian Ocean [*Gordon*, 2005], resulting in cooling of the

upper thermocline and intensification of the surface to upper thermocline temperature gradient in the TS outflow area. However, previous studies including modeling experiments suggested that the total transport of the ITF was reduced and shifted from the thermocline to the surface during the LGM [*Kuhnt et al.*, 2004; *Žuvela*, 2005; *Xu et al.*, 2008]. Thus, relatively warm and salty Indian Ocean upper thermocline waters dominated in the TS during the LGM, leading to a depressed ΔT between surface and thermocline waters, as indicated in Figure 6. Vertical mixing at locations exposed to monsoon wind-driven upwelling or typhoon tracks may have further depressed the upper ocean thermal gradient (ΔT) in the TS during the LGM. Today, seasonal upwelling develops during austral winter in the northern TS due to prevailing southeasterly monsoonal winds. During the LGM, extremely low ΔT in the TS (Figure 6) may have been due to wind-driven upwelling at locations, where glacially intensified monsoonal winds promoted intensified mixing of the upper water column [*Müller and Opdyke*, 2000; *Holbourn et al.*, 2005].

[41] Deglacial freshening of upper thermocline waters in the northern TS was most likely related to increasing freshwater influence from the Java Sea, altering the upper profile of the ITF downstream of the Makassar Strait. The surface to upper thermocline ΔT increased in all cores south of the Makassar Strait from the LGM to Holocene, reflecting shoaling of the thermocline (Figure 6). This shoaling trend was probably related to intensification of the ITF thermocline flow and reduction in the ITF surface component during the Holocene, once the Sunda shelf became flooded and freshwater influx from the SCS through the Karimata Strait resumed [*Xu et al.*, 2008]. In contrast, the SCS cores do not show such a pronounced change in upper ocean ΔT from the LGM to Holocene, and upper ocean waters remained relatively fresher and warmer than in the TS.

5. Conclusion

[42] Sea surface and upper thermocline temperature and salinity proxy data from twenty-four stations in the IPWP region indicate that a marked hydrological contrast prevailed between the SCS and the Indonesian Seas during the LGM (18–21.5 ka), early Holocene insolation maximum (8–9 ka) and late Holocene (0–2 ka). This regional contrast was particularly enhanced during the LGM, when the freshwater flux from the southern SCS through the Java Sea was shut off. The increase in SCS surface $\delta^{18}O_{sw\text{-}corr}$ from the LGM to late Holocene is attributed to resumption of freshwater export through the Java Sea after ~9.5 ka and to enhanced influx of NW Pacific waters into the SCS through the Luzon Strait. In the eastern Indian Ocean and TS, deglacial shoaling of the thermocline reflects intensification of the ITF subsurface component from the early to late Holocene. Increased freshwater export from the Java Sea fundamentally altered the vertical structure of the ITF from surface- to thermocline-dominated flow and led to substantial freshening of the TS and tropical Indian Ocean during the early Holocene. Glacial-interglacial $\delta^{18}O_{sw\text{-}corr}$ distribution over the IPWP region exhibits markedly different spatial patterns than modern El Niño related precipitation anomalies, indicating that ENSO variability cannot account for hydrological changes occurring over the IPWP from the LGM to late Holocene. We suggest that the shift in main exit portals for low-salinity waters out of the SCS from the Mindoro Strait and Luzon Strait to the Kalimata Strait had major repercussions for regional and global climate and circulation patterns during the Holocene.

[43] **Acknowledgments.** We thank Frank Bassinot, Thibault de Garidel-Thoron, and Yair Rosenthal for discussions and contributing data and Karin Kißling for technical help. Special thanks are given to Robert Thunell and Michael Sarnthein for providing sediment samples and to Timothé Bolliet and Zhimin Jian for sharing unpublished data. We are grateful to Editor Rainer Zahn and three reviewers for their insightful comments which greatly improved our manuscript. We extend our sincere thanks to the "SONNE-185" crew and shipboard scientific party for their dedicated efforts in recovering sediment cores from the Timor Sea. This work was funded by the Deutsche Forschungsgemeinschaft (DFG grant KU649/28-1) and the German Ministry of Education, Science and Technology (BMBF grant 03G0185A). Additional support for J. Xu came from the National Natural Science Foundation of China (grant 40906032) and a grant from the MOST Special Fund from the State Key Laboratory of Continental Dynamics, Northwest University, Xi'an, China.

References

Aleinov, I., and G. A. Schmidt (2006), Water isotopes in the GISS ModelE land surface scheme, *Global Planet. Change*, *51*, 108–120, doi:10.1016/j.gloplacha.2005.12.010.

Anand, P., H. Elderfield, and M. H. Conte (2003), Calibration of Mg/Ca thermometry in planktonic foraminifera from a sediment trap time series, *Paleoceanography*, *18*(2), 1050, doi:10.1029/2002PA000846.

Andreasen, D. J., and A. C. Ravelo (1997), Tropical Pacific Ocean thermocline depth reconstructions for the Last Glacial Maximum, *Paleoceanography*, *12*(3), 395–413, doi:10.1029/97PA00822.

Barker, S., I. Cacho, H. Benway, and K. Tachikawa (2005), Planktonic foraminiferal Mg/Ca as a proxy for past oceanic temperatures: A methodological overview and data compilation for the Last Glacial Maximum, *Quat. Sci. Rev.*, *24*, 821–834, doi:10.1016/j.quascirev.2004.07.016.

Barker, S., P. Diz, M. J. Vautravers, J. Pike, G. Knorr, I. R. Hall, and W. S. Broecker (2009), Interhemispheric Atlantic seesaw response during the last deglaciation, *Nature*, *457*, 1097–1102, doi:10.1038/nature07770.

Bemis, B. E., H. J. Spero, J. Bijma, and D. W. Lea (1998), Reevaluation of the oxygen isotopic composition of planktonic foraminifera: Experimental results and revised paleotemperature equations, *Paleoceanography*, *13*(2), 150–160, doi:10.1029/98PA00070.

Bjerknes, J. (1969), Atmospheric teleconnections from the equatorial Pacific, *Mon. Weather Rev.*, *97*, 163–172, doi:10.1175/1520-0493(1969)097<0163:ATFTEP>2.3.CO;2.

Butzin, M., M. Prange, and G. Lohmann (2005), Radiocarbon simulations for the glacial ocean: The effects of wind stress, Southern Ocean sea ice and Heinrich events, *Earth Planet. Sci. Lett.*, *235*, 45–61, doi:10.1016/j.epsl.2005.03.003.

Chen, G., C. Fang, C. Zhang, and Y. Chen (2004), Observing the coupling effect between warm pool and "rain pool" in the Pacific Ocean, *Remote Sens. Environ.*, *91*, 153–159, doi:10.1016/j.rse.2004.02.010.

Cheng, X., B. Huang, Z. Jian, Q. Zhao, J. Tian, and J. Li (2005), Foraminiferal isotopic evidence for monsoonal activity in the South China Sea: A present-LGM comparison, *Mar. Micropaleontol.*, *54*, 125–139, doi:10.1016/j.marmicro.2004.09.007.

Cléroux, C., E. Cortijo, J.-C. Duplessy, and R. Zahn (2007), Deep-dwelling foraminifera as thermocline temperature recorders, *Geochem. Geophys. Geosyst.*, *8*, Q04N11, doi:10.1029/2006GC001474.

Conan, S. M.-H., E. M. Ivanova, and G.-J. A. Brummer (2002), Quantifying carbonate dissolution and calibration of foraminiferal dissolution indices in the Somali Basin, *Mar. Geol.*, *182*, 325–349, doi:10.1016/S0025-3227(01)00238-9.

Dai, A., and T. M. L. Wigley (2000), Global patterns of ENSO-induced precipitation, *Geophys. Res. Lett.*, *27*, 1283–1286, doi:10.1029/1999GL011140.

Dekens, P. S., D. W. Lea, D. K. Pak, and H. J. Spero (2002), Core top calibration of Mg/Ca

in tropical foraminifera: Refining paleotemperature estimation, *Geochem. Geophys. Geosyst.*, *3*(4), 1022, doi:10.1029/2001GC000200.

de Villiers, S., M. Greaves, and H. Elderfield (2002), An intensity ratio calibration method for the accurate determination of Mg/Ca and Sr/Ca of marine carbonates by ICP-AES, *Geochem. Geophys. Geosyst.*, *3*(1), 1001, doi:10.1029/2001GC000169.

Fairbanks, R. G., R. A. Mortlock, T.-C. Chiu, L. Cao, A. Kaplan, T. P. Guilderson, T. W. Fairbanks, and A. L. Bloom (2005), Marine radiocarbon calibration curve spanning 10,000 to 50,000 years B.P. based on paired $^{230}Th/^{234}U/^{238}U$ and ^{14}C dates on pristine corals, *Quat. Sci. Rev.*, *24*, 1781–1796, doi:10.1016/j.quascirev.2005.04.007.

Farmer, E. C., A. Kaplan, P. B. de Menocal, and J. Lynch-Stieglitz (2007), Corroborating ecological depth preferences of planktonic foraminifera in the tropical Atlantic with the stable oxygen isotope ratios of core top specimens, *Paleoceanography*, *22*, PA3205, doi:10.1029/2006PA001361.

Fleitmann, D., et al. (2007), Holocene ITCZ and Indian monsoon dynamics recorded in stalagmites from Oman and Yemen (Socotra), *Quat. Sci. Rev.*, *26*, 170–188, doi:10.1016/j.quascirev.2006.04.012.

Gordon, A. L. (2005), The Indonesian Seas: Oceanography of the Indonesian Seas and their Throughflow, *Oceanography*, *18*(4), 14–27.

Gordon, A. L., and R. A. Fine (1996), Pathways of water between the Pacific and Indian oceans in the Indonesian seas, *Nature*, *379*, 146–149, doi:10.1038/379146a0.

Gordon, A. L., R. D. Susanto, and K. Vranes (2003), Cool Indonesian throughflow as a consequence of restricted surface layer flow, *Nature*, *425*, 824–828, doi:10.1038/nature02038.

Haug, G. H., K. A. Hughen, D. M. Sigman, L. C. Peterson, and U. Röhl (2001), Southward migration of the Intertropical Convergence Zone through the Holocene, *Science*, *293*, 1304–1308, doi:10.1126/science.1059725.

Holbourn, A., W. Kuhnt, H. Kawamura, Z. Jian, P. Grootes, H. Erlenkeuser, and J. Xu (2005), Orbitally paced paleoproductivity variations in the Timor Sea and Indonesian Throughflow variability during the last 460 kyr, *Paleoceanography*, *20*, PA3002, doi:10.1029/2004PA001094.

Huang, B. (2002), Late Plio-Pleistocene evolution of the East Asian monsoon recorded by foraminiferal fauna in the northern South China Sea (in Chinese with English abstract), Ph.D. thesis, 48 pp., Tongji Univ., Shanghai, China.

Huang, K.-F., C.-F. You, H.-L. Lin, and Y.-T. Shieh (2008), In situ calibration of Mg/Ca ratio in planktonic foraminiferal shell using time series sediment trap: A case study of intense dissolution artifact in the South China Sea, *Geochem. Geophys. Geosyst.*, *9*, Q04016, doi:10.1029/2007GC001660.

Jian, Z., P. Wang, M.-P. Chen, and B. Li (2000), Foraminiferal responses to major Pleistocene paleoceanographic changes in the southern South China Sea, *Paleoceanography*, *15*(2), 229–243, doi:10.1029/1999PA000431.

Kienast, M., S. Steinke, K. Stattegger, and S. E. Calvert (2001), Synchronous tropical South China Sea SST change and Greenland warming during deglaciation, *Science*, *297*, 226–230.

Kisakürek, B., A. Eisenhauer, F. Böhm, D. Garbe-Schönberg, and J. Erez (2008), Controls on shell Mg/Ca and Sr/Ca in cultured planktonic foraminiferan, *Globigerinoides ruber* (white), *Earth Planet. Sci. Lett.*, *273*, 260–269, doi:10.1016/j.epsl.2008.06.026.

Koutavas, A., J. Lynch-Stieglitz, T. M. Marchitto Jr., and J. P. Sachs (2002), El Niño-like pattern in ice age tropical Pacific sea surface temperature, *Science*, *297*, 226–230, doi:10.1126/science.1072376.

Kuhnt, W., A. Holbourn, R. Hall, M. Žuvela, and R. Käse (2004), Neogene history of the Indonesian Throughflow, in *Continent-Ocean Interactions Within East Asia Marginal Seas*, *Geophys. Monogr. Ser.*, vol. 149, edited by P. Clift et al., pp. 299–320, AGU, Washington, D. C.

Lambeck, K., and J. Chappell (2001), Sea level change through the last glacial cycle, *Science*, *292*, 679–686, doi:10.1126/science.1059549.

Le, J., and N. J. Shackleton (1992), Carbonate dissolution fluctuations in the western equatorial Pacific during the late Quaternary, *Paleoceanography*, *7*, 21–42, doi:10.1029/91PA02854.

Lea, D. W., D. K. Pak, and H. J. Spero (2000), Climate impact of late Quaternary equatorial Pacific sea surface temperature variations, *Science*, *289*, 1719–1724, doi:10.1126/science.289.5485.1719.

Lee, T., I. Fukumori, D. Menemenlis, Z. Xing, and L.-L. Fu (2002), Effects of the Indonesian Throughflow on the Pacific and Indian oceans, *J. Phys. Oceanogr.*, *32*(5), 1404–1429, doi:10.1175/1520-0485(2002)032<1404:EOTITO>2.0.CO;2.

Linsley, B. K., Y. Rosenthal, and D. W. Oppo (2010), Holocene evolution of the Indonesian throughflow and the western Pacific warm pool, *Nat. Geosci.*, *3*, 578–583, doi:10.1038/ngeo920.

Liu, Z., J. Kutzbach, and L. Wu (2000), Modeling climate shift of El Nino variability in the Holocene, *Geophys. Res. Lett.*, *27*(15), 2265–2268, doi:10.1029/2000GL011452.

Liu, Z., S. P. Harrison, J. Kutzbach, and B. Otto-Bliesner (2004), Global monsoons in the mid-Holocene and oceanic feedback, *Clim. Dyn.*, *22*, 157–182, doi:10.1007/s00382-003-0372-y.

Locarnini, R. A., A. V. Mishonov, J. I. Antonov, T. P. Boyer, and H. E. Garcia (2006), *World Ocean Atlas 2005*, vol. 1, *Temperature, NOAA Atlas NESDIS*, vol. 61, edited by S. Levitus, 182 pp., NOAA, Silver Spring, Md.

Loubere, P., M. Richaud, Z. Liu, and F. Mekik (2003), Oceanic conditions in the eastern equatorial Pacific during the onset of ENSO in the Holocene, *Quat. Res.*, *60*, 142–148, doi:10.1016/S0033-5894(03)00092-9.

Martin, P. A., and D. W. Lea (2002), A simple evaluation of cleaning procedures on fossil benthic foraminiferal Mg/Ca, *Geochem. Geophys. Geosyst.*, *3*(10), 8401, doi:10.1029/2001GC000280.

Marx, S. K., H. A. McGowan, and B. S. Kamber (2009), Long-range dust transport from eastern Australia: A proxy for Holocene aridity and ENSO-type climate variability, *Earth Planet. Sci. Lett.*, *282*, 167–177, doi:10.1016/j.epsl.2009.03.013.

Mathien-Blard, E., and F. Bassinot (2009), Salinity bias on the foraminifera Mg/Ca thermometry: Correction procedure and implications for past ocean hydrographic reconstructions, *Geochem. Geophys. Geosyst.*, *10*, Q12011, doi:10.1029/2008GC002353.

Mohtadi, M., S. Steinke, J. Groeneveld, H. T. G. Fink, T. Rixen, D. Hebbeln, B. Donner, and B. Herunadi (2009), Low-latitude control on seasonal and interannual changes in plaktonic foraminferal flux and shell geochemistry off south Java: A sediment trap study, *Paleoceanography*, *24*, PA1201, doi:10.1029/2008PA001636.

Moy, C. M., G. O. Seltzer, D. T. Rodbell, and D. M. Anderson (2002), Variability of El Niño/Southern Oscillation activity at millennial timescales during the Holocene epoch, *Nature*, *420*, 162–165, doi:10.1038/nature01194.

Müller, A., and B. N. Opdyke (2000), Glacial-interglacial changes in nutrient utilization and paleoproductivity in the Indonesian Throughflow sensitive Timor Trough, easternmost Indian Ocean, *Paleoceanography*, *15*, 85–94, doi:10.1029/1999PA900046.

Ni, Y., G. L. Foster, T. Bailey, T. Elliott, D. N. Schmidt, P. Pearson, B. Haley, and C. Coath (2007), A core top assessment of proxies for the ocean carbonate system in surface-dwelling foraminifers, *Paleoceanography*, *22*, PA3212, doi:10.1029/2006PA001337.

Oppo, D. W., and Y. Sun (2005), Amplitude and timing of sea-surface temperature change in the northern South China Sea: Dynamic link to the East Asian monsoon, *Geology*, *33*(10), 785–788, doi:10.1130/G21867.1.

Oppo, D. W., B. K. Linsley, Y. Rosenthal, S. Dannenmann, and L. Beaufort (2003), Orbital and suborbital climate variability in the Sulu Sea, western tropical Pacific, *Geochem. Geophys. Geosyst.*, *4*(1), 1003, doi:10.1029/2001GC000260.

Oppo, D. W., Y. Rosenthal, and B. K. Linsley (2009), 2,000-year-long temperature and hydrology reconstructions from the Indo-Pacific warm pool, *Nature*, *460*, 1113–1116, doi:10.1038/nature08233.

Pierrehumbert, R. T. (2000), Climate change and the Tropical Pacific: The Sleeping Dragon Wakes, *Proc. Natl. Acad. Sci. U. S. A.*, *97*, 1355–1358, doi:10.1073/pnas.97.4.1355.

Potemra, J. T., S. L. Hautala, and J. Sprintall (2003), Vertical structure of Indonesian throughflow in a large-scale model, *Deep Sea Res., Part II*, *50*, 2143–2161, doi:10.1016/S0967-0645(03)00050-X.

Qu, T., Y. T. Song, and T. Yamagata (2009), An introduction to the South China Sea throughflow: Its dynamics, variability, and application for climate, *Dyn. Atmos. Oceans*, *47*, 3–14, doi:10.1016/j.dynatmoce.2008.05.001.

Regenberg, M., S. Steph, D. Nürnberg, R. Tiedemann, and D. Garbe-Schönberg (2009), Calibrating Mg/Ca ratios of multiple planktonic foraminiferal species with $\delta^{18}O$-calcification temperatures: Paleothermometry for the upper water column, *Earth Planet. Sci. Lett.*, *278*, 324–336, doi:10.1016/j.epsl.2008.12.019.

Rodbell, D. T., G. O. Seltzer, D. M. Anderson, M. B. Abbott, D. B. Enfield, and J. H. Newman (1999), An ~15,000-year record of El Niño-driven alleviation in southwestern Ecuador, *Science*, *283*, 516–520, doi:10.1126/science.283.5401.516.

Rosenthal, Y., and G. P. Lohmann (2002), Accurate estimation of sea surface temperatures using dissolution-corrected calibrations for Mg/Ca paleothermometry, *Paleoceanography*, *17*(3), 1044, doi:10.1029/2001PA000749.

Rosenthal, Y., D. W. Oppo, and B. K. Linsley (2003), The amplitude and phasing of climate change during the last deglaciation in the Sulu Sea, western equatorial Pacific, *Geophys. Res. Lett.*, *30*(8), 1428, doi:10.1029/2002GL016612.

Rosenthal, Y., et al. (2004), Interlaboratory comparison study of Mg/Ca and Sr/Ca measure-

ments in planktonic foraminifera for paleoceanographic research, *Geochem. Geophys. Geosyst.*, *5*(4), Q04D09, doi:10.1029/2003GC000650.

Sandweiss, D. H., K. A. Maasch, R. L. Burger, J. B. Richardson III, H. B. Rollins, and A. Clement (2001), Variation in Holocene El Niño frequencies: Climate records and cultural consequences in ancient Peru, *Geology*, *29*(7), 603–606, doi:10.1130/0091-7613(2001)029<0603:VIHENO>2.0.CO;2.

Sarnthein, M., R. Gersonde, S. Niebler, U. Pflaumann, R. Spielhagen, J. Thiede, G. Wefer, and M. Weinelt (2003), Overview of Glacial Atlantic Ocean Mapping (GLAMAP 2000), *Paleoceanography*, *18*(2), 1030, doi:10.1029/2002PA000769.

Sarnthein, M., P. M. Grootes, J. P. Kennett, and M.-J. Nadeau (2007), ^{14}C reservoir ages show deglacial changes in ocean currents and carbon cycle, in *Past and Future Changes of the Oceanic Meridional Overturning Circulation: Mechanisms and Impacts*, *Geophys. Monogr. Ser.*, vol. 173, edited by A. Schmittner, J. C. H. Chiang, and S. Hemmings, pp. 175–196, AGU, Washington, D. C., doi:10.1029/173GM13.

Schleicher, M., P. M. Grootes, M. J. Nadeau, and A. Schoon (1998), The carbonate ^{14}C background and its components at the Leibniz AMS facility, *Radiocarbon*, *40*, 85–93.

Stott, L., C. Poulsen, S. Lund, and R. Thunell (2002), Super ENSO and global climate oscillations at millennial time scales, *Science*, *297*, 222–226, doi:10.1126/science.1071627.

Stott, L., K. Cannariato, R. Thunell, G. H. Haug, A. Koutavas, and S. Lund (2004), Decline of surface temperature and salinity in the western tropical Pacific Ocean in the Holocene epoch, *Nature*, *431*, 56–59, doi:10.1038/nature02903.

Stott, L., A. Timmerman, and R. Thunell (2007), Southern Hemisphere and deep-sea warming led deglacial atmospheric CO_2 rise and tropical warming, *Science*, *318*, 435–438, doi:10.1126/science.1143791.

Tachikawa, K., S. Sépulcre, T. Toyofuku, and E. Bard (2008), Assessing influence of diagenetic carbonate dissolution on planktonic foraminiferal Mg/Ca in the southeastern Arabian Sea over the past 450 ka: Comparison between *Globigerinoides ruber* and *Globigerinoides sacculifer*, *Geochem. Geophys. Geosyst.*, *9*, Q04037, doi:10.1029/2007GC001904.

Tachikawa, K., L. Vidal, C. Sonzogni, and E. Bard (2009), Glacial/interglacial sea surface temperature changes in the southwest Pacific ocean over the past 360 ka, *Quat. Sci. Rev.*, *28*, 1160–1170, doi:10.1016/j.quascirev.2008.12.013.

Tierney, J. E., and J. M. Russell (2007), Abrupt climate change in southeast tropical Africa influenced by Indian monsoon variability and ITCZ migration, *Geophys. Res. Lett.*, *34*, L15709, doi:10.1029/2007GL029508.

Tierney, J. E., D. W. Oppo, Y. Rosenthal, J. M. Russell, and B. K. Linsley (2010), Coordinated hydrological regimes in the Indo-Pacific region during the past two millennia, *Paleoceanography*, *25*, PA1102, doi:10.1029/2009PA001871.

Tozuka, T., T. Qu, and T. Yamagata (2007), Dramatic impact of the South China Sea on the Indonesian Throughflow, *Geophys. Res. Lett.*, *34*, L12612, doi:10.1029/2007GL030420.

Tozuka, T., T. Qu, Y. Masumoto, and T. Yamagata (2009), Impacts of the South China Sea Throughflow on seasonal and interannual variations of the Indonesian Throughflow, *Dyn. Atmos. Oceans*, *47*, 73–85, doi:10.1016/j.dynatmoce.2008.09.001.

Visser, K., R. Thunell, and L. Stott (2003), Magnitude and timing of temperature change in the Indo-Pacific warm pool during deglaciation, *Nature*, *421*, 152–155, doi:10.1038/nature01297.

Vranes, K., A. L. Gordon, and A. Ffield (2002), The heat transport of the Indonesian throughflow and implications for the Indian Ocean heat budget, *Deep Sea Res., Part II*, *49*(7–8), 1391–1410, doi:10.1016/S0967-0645(01)00150-3.

Waelbroeck, C., L. Labeyrie, E. Michel, J. C. Duplessy, J. F. McManus, K. Lambeck, E. Balbon, and M. Labracherie (2002), Sea-level and deep water temperature changes derived from benthic foraminifera isotopic records, *Quat. Sci. Rev.*, *21*, 295–305, doi:10.1016/S0277-3791(01)00101-9.

Wang, L., M. Sarnthein, H. Erlenkeuser, J. Grimalt, P. Grootes, S. Heilig, E. Ivanova, M. Kienast, C. Pelejero, and U. Pflaumann (1999), East Asian monsoon climate during the late Pleistocene: High-resolution sediment records from the South China Sea, *Mar. Geol.*, *156*, 245–284, doi:10.1016/S0025-3227(98)00182-0.

Webb, R. S., D. H. Rind, S. J. Lehmann, R. J. Healy, and D. Siegmann (1997), Influence of ocean heat transport on the climate of the Last Glacial Maximum, *Nature*, *385*, 695–699, doi:10.1038/385695a0.

Wei, G.-Y., T.-C. Chiu, and Y.-G. Chen (2003), Toward establishing a maritime proxy record of the East Asian summer monsoons for the late Quaternary, *Mar. Geol.*, *201*, 67–79, doi:10.1016/S0025-3227(03)00209-3.

Wells, L. E. (1990), Holocene history of the El Niño phenomenon as recorded in flood sediments of northern coastal Peru, *Geology*, *18*, 1134–1137, doi:10.1130/0091-7613(1990)018<1134:HHOTEN>2.3.CO;2.

Xu, J. (2004), Quaternary planktonic foraminiferal assemblages in the southern South China Sea and paleoclimatic variations, Ph.D. thesis, School of Ocean and Earth Sci., Tongji Univ., Shanghai, China.

Xu, J., W. Kuhnt, A. Holbourn, N. Andersen, and G. Bartoli (2006), Changes in the vertical profile of the Indonesian Throughflow during Termination II: Evidence from the Timor Sea, *Paleoceanography*, *21*, PA4202, doi:10.1029/2006PA001278.

Xu, J., A. Holbourn, W. Kuhnt, Z. Jian, and H. Kawamura (2008), Changes in the thermocline structure of the Indonesian outflow during Terminations I and II, *Earth Planet. Sci. Lett.*, *273*, 152–162, doi:10.1016/j.epsl.2008.06.029.

Yancheva, G., N. R. Nowaczyk, J. Mingram, P. Dulski, G. Schettler, J. F. W. Negendank, J. Q. Liu, D. M. Sigman, L. C. Peterson, and G. H. Haug (2007), Influence of the intertropical convergence zone on the East Asian monsoon, *Nature*, *445*, 74–77, doi:10.1038/nature05431.

Yuan, D. X., et al. (2004), Timing, duration, and transitions of the last interglacial Asian monsoon, *Science*, *304*, 575–578, doi:10.1126/science.1091220.

Zuraida, R., A. Holbourn, D. Nürnberg, W. Kuhnt, A. Dürkop, and A. Erichsen (2009), Evidence for Indonesian Throughflow slowdown during Heinrich events 3–5, *Paleoceanography*, *24*, PA2205, doi:10.1029/2008PA001653.

Žuvela, M. (2005), Modelling of the Indonesian Throughflow on glacial-interglacial timescales, Ph.D. thesis, Math.-Naturwiss. Fakul., Christian-Albrechts-Univ., Kiel, Germany.

N. Andersen, Leibniz Laboratory for Radiometric Dating and Stable Isotope Research, Christian Albrechts University, Max-Eyth-Strasse 11-13, D-24118 Kiel, Germany. (nandersen@leibniz.uni-kiel.de)

A. Holbourn, W. Kuhnt, and M. Regenberg, Institute of Geosciences, Christian Albrechts University, Olshausenstr. 40, D-24118 Kiel, Germany. (ah@gpi.uni-kiel.de; wk@gpi.uni-kiel.de; regenberg@gpi.uni-kiel.de)

J. Xu, Department of Geology, Northwest University, 229 North Taibai Rd., Xi'an, Shaanxi 710069, China. (jx08@live.cn)